Chiral Carbon Nanocables

International Edition: DOI: 10.1002/anie.201605354
German Edition: DOI: 10.1002/ange.201605354

Formation of Coaxial Nanocables with Amplified Supramolecular Chirality through an Interaction between Carbon Nanotubes and a Chiral π-Gelator

*Balaraman Vedhanarayanan, Vishnu S. Nair, Vijayakumar C. Nair, and Ayyappanpillai Ajayaghosh**

Dedicated to Professor Takuzo Aida on the occasion his 60th birthday

Abstract: *In an attempt to gather experimental evidence for the influence of carbon allotropes on supramolecular chirality, we found that carbon nanotubes (CNTs) facilitate amplification of the molecular chirality of a π-gelator (**MC-OPV**) to supramolecular helicity at a concentration much lower than that required for intermolecular interaction. For example, at a concentration 1.8×10^{-4} M, **MC-OPV** did not exhibit a CD signal; however, the addition of 0–0.6 mg of SWNTs resulted in amplified chirality as evident from the CD spectrum. Surprisingly, AFM analysis revealed the formation of thick helical fibers with a width of more than 100 nm. High-resolution TEM analysis and solid-state UV/Vis/NIR spectroscopy revealed that the thick helical fibers were cylindrical cables composed of individually wrapped and coaxially aligned SWNTs. Such an impressive effect of CNTs on supramolecular chirality and cylindrical-cable formation has not been reported previously.*

Handedness is a fascinating phenomenon observed in nature, from tiny organisms, such as tobacco mosaic virus, to massive asymmetric objects, such as galaxies.[1] Nature exploits various factors, such as the movement of solar light, the rotation of planets, and terrestrial magnetism, to regulate the chirality of nano-, micro-, and macrostructures present in the universe.[2] A lot of naturally occurring matter also assists the evolution of helical objects.[2a] For example, dust particles present in the atmosphere and in outer space may influence the handedness of micro- and macroscopic objects. Spontaneous chiral crystallization of certain small molecules under certain laboratory conditions is another example of an external influence on chirality.[3] Allotropes of carbon, such as carbon particles, C_{60}, C_{70}, and carbon nanotubes (CNTs), that are present in the atmosphere may also have a similar influence upon the helical organization of macroscopic objects of biological origin.[4] Previous studies have revealed that the interaction of CNTs with polymers, π-conjugated molecules, proteins, and DNA can result in functional hybrid materials with fascinating properties.[5] For example, CNTs significantly improve the stability of π-gelators and are known to impart intriguing properties to the resulting hybrid materials.[6] However, no reports are available to prove the influence of carbon allotropes on the evolution of supramolecular chirality, although small amounts of chiral π-systems are known to induce and amplify chirality when mixed with large amounts of self-assembling achiral systems.[7] Herein, we reveal that the interaction of CNTs with a chiral π-system has a strong influence on the amplification of molecular chirality into supramolecular helicity. Furthermore, we report the unprecedented formation of cylindrical nanocables comprising isolated and coaxially aligned single-walled carbon nanotubes (SWNTs).

For our studies, we selected a monocholesterol-appended OPV gelator, **MC-OPV**, which is known to form helical tapes

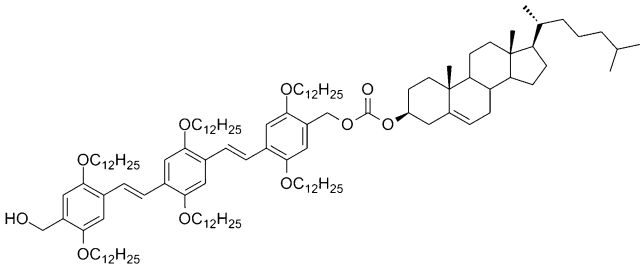

MC-OPV

upon self-assembly.[8] Up to a concentration of 1.8×10^{-4} M in *n*-decane, this molecule does not aggregate, as evident from its absorption and circular dichroism (CD) spectra, which exhibit the presence of the monomer species only (λ_{max} = 402 nm; Figure 1a). Interestingly, when small amounts of SWNTs (0.05–0.6 mg) were added to a solution of **MC-OPV** in *n*-decane, followed by sonication for 1–2 min, an additional shoulder band around 470 nm appeared, indicating the aggregation of the molecule. Furthermore, the appearance of van Hove singularities of the isolated CNTs in the UV/Vis/NIR absorption spectrum in the wavelength region of 550–1400 nm indicated the unbundling and dispersion of the nanotubes[9] (Figure 1c). The addition of the SWNTs induced a decrease in the emission intensities at 458 and 485 nm of the monomers, with the appearance of a broad emission band

[*] B. Vedhanarayanan, V. S. Nair, Dr. V. C. Nair, Prof. Dr. A. Ajayaghosh
Photosciences and Photonics Section, Chemical Sciences and Technology Division and Academy of Scientific and Innovative Research (AcSIR), CSIR-National Institute for Interdisciplinary Science and Technology (CSIR-NIIST)
Thiruvananthapuram 695 019 (India)
E-mail: ajayaghosh@niist.res.in

Supporting information and the ORCID identification numbers for the authors of this article can be found under: http://dx.doi.org/10.1002/anie.201605354.

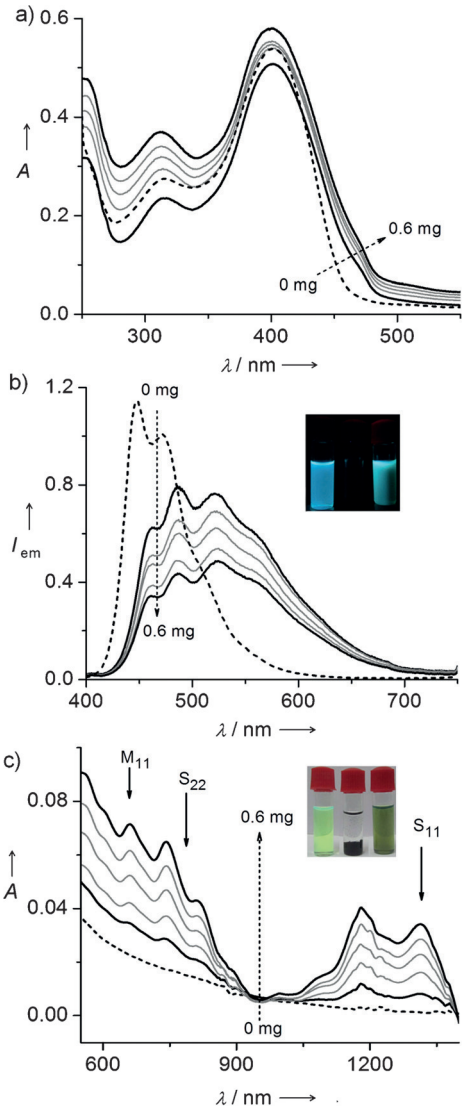

Figure 1. a) UV/Vis absorption spectra, b) fluorescence spectra, and c) Vis/NIR absorption spectra (550–1400 nm) of **MC-OPV** ($c = 1.8 \times 10^{-4}$ M, $l = 1$ mm, $\lambda_{ex} = 380$ nm) in the absence (dotted line) and presence (solid lines) of SWNTs. Insets: Photographs of **MC-OPV**, SWNTs, and the **MC-OPV/SWNT** hybrid in *n*-decane (left to right) under UV light (b) and ambient light (c).

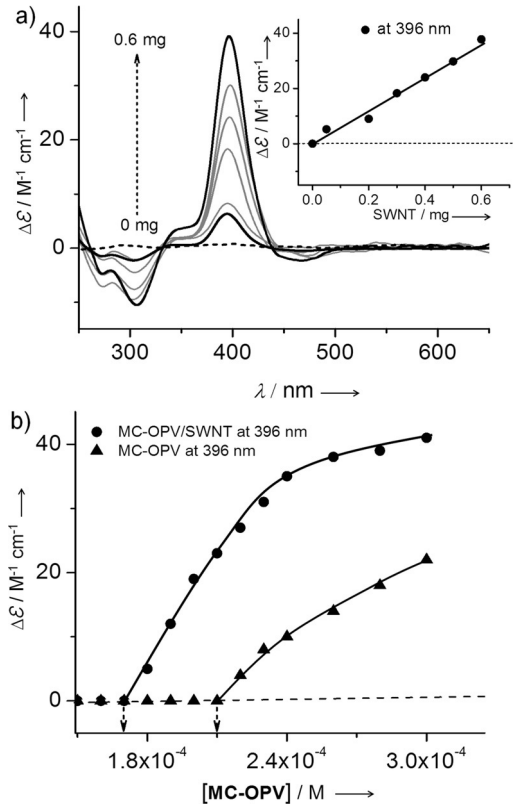

Figure 2. a) CD spectra of **MC-OPV** ($c = 1.8 \times 10^{-4}$ M) in *n*-decane with an increasing amount of SWNTs (0–0.6 mg). The corresponding change in the CD intensity with respect to the amount of SWNTs is shown in the inset. b) Change in CD intensity with increasing concentration of **MC-OPV** in the presence of 0.2 mg of SWNTs in *n*-decane.

corresponding to the aggregates at 550 nm (Figure 1b). As a result, the cyan emission of the solution turned a greenish-cyan color (inset of Figure 1b).

The CD spectrum of the gelator on the addition of SWNTs indicated the helical arrangement of the molecules. To be more precise, initially no CD signal was observed for **MC-OPV** at a 1.8×10^{-4} M concentration in *n*-decane, since at this concentration the molecule does not induce helical organization (Figure 2a). However, the addition of 0.05 mg of SWNTs resulted in a weak CD signal at 396 nm ($6\ M^{-1}\,cm^{-1}$; dissymmetry factor, $g_{396} = 1.24 \times 10^{-4}$), thus indicating a helical packing of the molecule. Upon further addition of SWNTs, the intensity of the CD signal gradually increased (inset of Figure 2a). For example, the addition of 0–0.6 mg of SWNTs to a solution of **MC-OPV** (concentration kept constant at 1.8×10^{-4} M) led a linear increase with a maximum CD intensity of $38\ M^{-1}\,cm^{-1}$. No enhancement in the CD signal was seen on the further addition of SWNTs. In the absence of SWNTs, the gelator did not show any CD signal up to a concentration of 2.0×10^{-4} M. However, an enhancement of the CD signal by a factor of nearly 23 was observed at the same concentration upon the addition of 0.2 mg of SWNTs. To observe the same CD intensity in the absence of SWNTs, the gelator concentration had to be increased to above 2.0×10^{-4} M, thus underlining the role of SWNTs in chirality amplification. The interaction between the gelator molecules and the CNTs involves H-bonding, van der Waals forces, and π-stacking.[6,8]

A variable-temperature study exhibited a decrease in the absorption (see Figure S1 in the Supporting Information), emission (see Figure S2a) and CD spectral intensities (see Figure S2b) of aggregates upon heating. The CD intensity of the **MC-OPV/SWNT** hybrid diminished during heating up to 40 °C, owing to the disassembly of the helical aggregates into the monomer species (see Figure S2b). Fitting of the parameters (see Figure S3a) revealed that the self-assembly process follows a cooperative mechanism.[10] Thermodynamic parameters, such as the elongation temperature (T_e), melting temperature (T_m), and enthalpy change (ΔH) of the **MC-OPV/SWNT** hybrid were calculated from the fitting curves obtained from the variable-temperature CD studies (see

Table S1 in the Supporting Information). The elongation temperature of the supramolecular aggregates of **MC-OPV** was 288 K in the presence of 0.2 mg of SWNTs, whereas it increased up to 294 K with 0.6 mg of SWNTs (see Figure S3b). The increase in the elongation temperature implies that the self-assembly process starts at even higher temperatures in the presence of SWNTs. Similarly, the melting temperatures of the aggregates were found to increase with increasing amounts of SWNTs. The higher melting temperatures indicate that SWNTs not only amplify the supramolecular chirality but also enhance the stability of the aggregates.

Raman spectral changes of the SWNTs and **MC-OPV/SWNT** are shown in Figure 3. They reveal a strong interaction of **MC-OPV** with the surface of SWNTs. The radial breathing

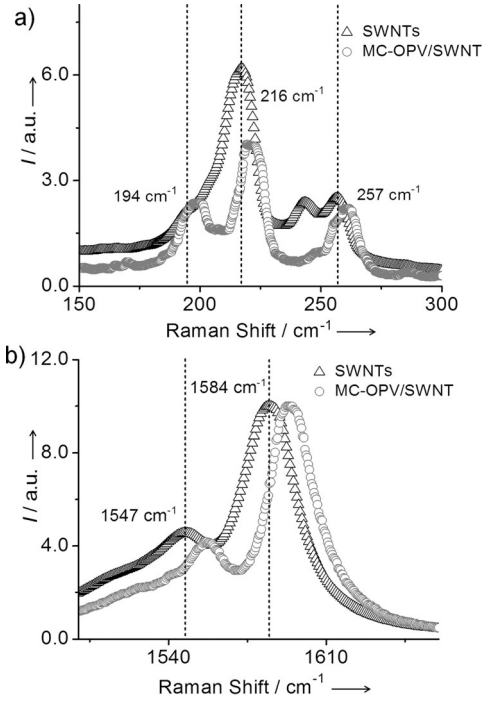

Figure 3. Raman spectra of SWNTs and **MC-OPV/SWNT** in a) the RBM region and b) the G-band region.

mode (RBM) region of the pristine SWNTs showed peaks at 194, 216, 242, and 257 cm^{-1}. In the case of the **MC-OPV/SWNT** hybrid, the peak at 194 cm^{-1} was shifted to 198 cm^{-1}. Similarly, the peaks at 216, 242, and 257 cm^{-1} were shifted to 220, 245, and 261 cm^{-1} with an upshift of 4, 3, and 4 cm^{-1}, respectively. The G-band of the SWNTs at 1584 cm^{-1} was also shifted to 1593 cm^{-1}. The upshift of the peaks of **MC-OPV/SWNT** could be attributed to the unbundling of SWNTs by **MC-OPV** as well as the pressure exerted by the helically wrapped supramolecular tape of **MC-OPV** around the SWNT surface.

AFM images of **MC-OPV** indicate the formation of helical fibers of 50–150 nm in width with a helical pitch of 50–80 nm (Figure 4a; see also Figure S7). However, the heights of the fibers were in the range of 4–6 nm, thus indicating that they are very thin. On the other hand, the **MC-OPV/SWCNT** mixture showed densely aggregated thin fibers (width of 20–100 nm) that are bundled to form superstructures of SWNTs helically wrapped with **MC-OPV** (more than 100 nm width; Figure 4b; see also Figure S8). The hybrid fibers showed a right-handed helical pitch (100–200 nm) in most cases. Since the UV/Vis/NIR absorption spectrum showed the dispersion of CNTs upon interaction with **MC-OPV**, thus indicating the debundling of the former, the observation of superfibers of more than 100 nm in width was a surprise.

The inset in Figure 4b shows an isolated helical superstructure with a width of 90 nm. Interestingly, the section analysis of the superfiber showed a height of 60 nm, which is nearly 10 times more than that of the **MC-OPV** fibers, thus indicating a cylindrical morphology for the hybrid assembly. Since the size of each SWNT is approximately 1 nm, the formation of such large cylindrical fibers can be explained in two different ways: wrapping of **MC-OPV** onto the bundled CNTs, or rebundling of the individual CNTs wrapped by **MC-OPV** and subsequent wrapping by **MC-OPV** upon evaporation on the mica substrate. If the superstructures are formed through the former route, one should not see the van Hove singularity of the individual CNTs. In contrast, if the superstructures are formed through the latter route, the UV/Vis/NIR absorption spectrum of the hybrid material should show the van Hove fine structure of the SWNTs.

To investigate this hypothesis, we measured the solid-state UV/Vis/NIR absorption spectrum of a **MC-OPV/SWNT** hybrid film, which exhibited the van Hove singularity (Figure 5). This observation supports the formation of superstructures by the latter route, in which the CNTs are separated from one another by the helically wrapped **MC-OPV**, a structure further established by TEM analysis of **MC-OPV/SWNT** (Figure 4c,d; see also Figure S9). High-resolution TEM (HRTEM) images of a large (ca. 25 nm) and a small (ca. 10 nm) cylindrical cable indicate the presence of aligned SWNTs in the supercoiled fibers. We also observed aggregated superhelical fibers of more than 100 nm in width (see Figure S9d and inset), which are coincident with the AFM images (Figure 4b; see also Figure S8). The intensity histograms of the HRTEM images reveal that the individual CNTs are closely bound in the pristine SWNTs, with an average intertubular distance of (0.66 ± 0.05) nm (see Figure S10), whereas when they are individually wrapped by **MC-OPV** and aligned in the supercoiled fibers of **MC-OPV/SWNT**, the average intertubular distance is increased to $(0.8–0.9 \pm 0.05)$ nm (inset of Figure 4c,d).

On the basis of the above experimental data, we propose the formation of coaxial cylindrical cables of SWNTs as shown in Figure 6. In solution, SWNTs interact with **MC-OPV** to form helically wrapped individual nanotubes. Drop casting of the wrapped nanotubes on substrates, followed by evaporation of the solvent, results in rebundling of the individually wrapped CNTs, which are further wrapped with **MC-OPV** to form cylindrical cables of more than 100 nm in width with aligned CNTs. When multiwalled carbon nanotubes (MWNTs) were used instead of SWNTs, the intensities of the CD signals were relatively weak (see Figure S4), since the total surface area available for SWNTs is much higher than that of the same amount of MWNTs. We also studied the

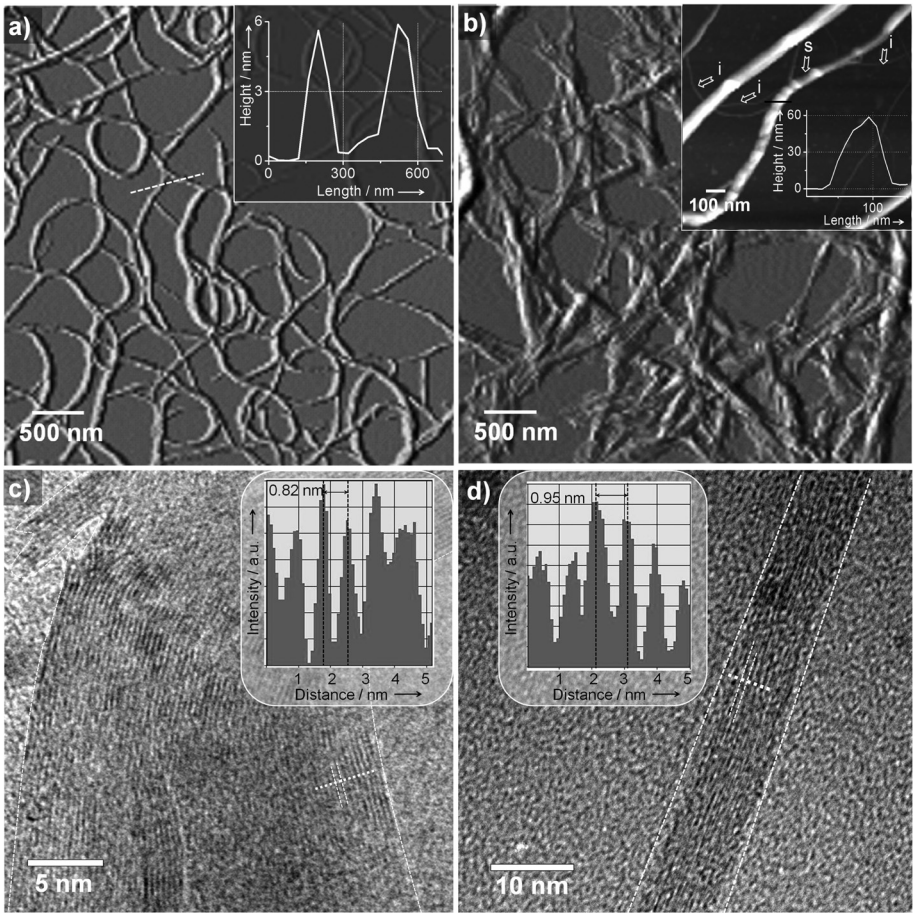

Figure 4. a) AFM magnitude images of **MC-OPV** (a) and the **MC-OPV/SWNT** hybrid (b). The inset of (a) shows the height profile for the marked region. The inset of (b) shows the AFM height image of individually wrapped (marked by symbol "I") and supercoiled fibers (marked by symbol "s") of the hybrid along with the height profile of a supercoiled fiber at the marked position (black line). c, d) HRTEM images of the cylindrical cables of **MC-OPV/SWNT**, drop cast from *n*-decane solution ($c = 1.8 \times 10^{-4}$ M). Insets show intensity histograms for the marked regions.

effect of CNTs on two other OPV gelators (see the Supporting Information), which also exhibited chirality amplification, but to a lesser extent (see Figures S5d and S6d). Further studies on the interaction of CNTs with different types of π-gelators, to generalize the effect on chirality and coaxial-cable formation, are in progress.

In summary, we have presented experimental evidence for the influence of CNTs on chirality amplification in molecular assemblies, as illustrated with a chiral π-gelator. The extent of chirality amplification depends upon the strength of the interaction of the gelator with CNTs as well as the strength of gelator aggregation. MWNTs exhibited relatively weak chirality amplification as compared to that of SWNTs, owing to the lower surface area of the former that is available for the gelator interaction. Detailed UV/Vis/NIR, AFM, and TEM analysis of the hybrid revealed an interesting morphological feature, in which each nanotube is site-isolated to form coaxially aligned cylindrical cables. Such alignment of nanotubes without any external force is a unique example of nanotube self-alignment and can be exploited for making hybrids with intriguing physical properties.

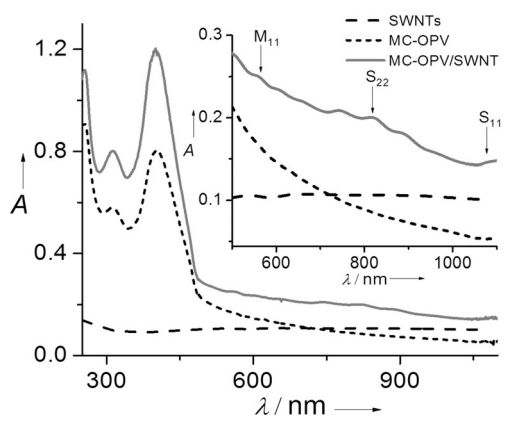

Figure 5. Solid-state (film) UV/Vis/NIR absorption spectra of SWNTs, **MC-OPV**, and **MC-OPV/SWNT**. The inset shows the zoomed area between 550 and 1200 nm.

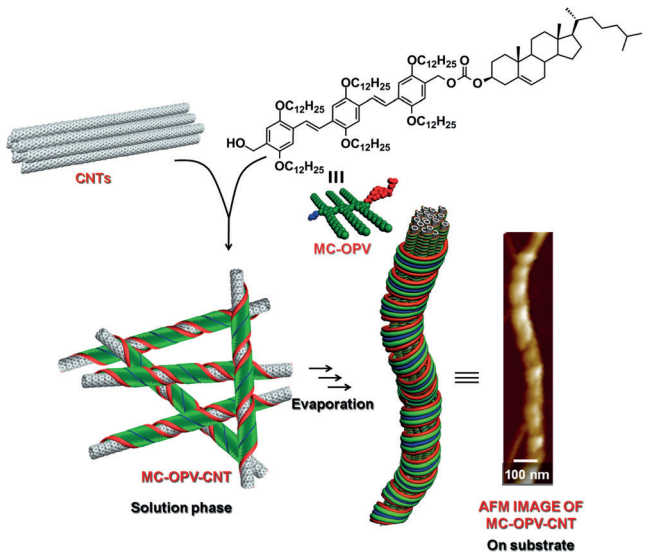

Figure 6. Schematic representation of the formation of coaxial cylindrical nanocables of CNTs by helically wrapped π-gelators, thus leading to chirality amplification.

Acknowledgements

We thank the CSIR, Government of India, for financial support, Kiran Mohan (CSIR-NIIST) for TEM analysis, and Aswin Maheswar (CSIR-NIIST) for AFM analysis. A.A. is grateful to the DST-SERB, Government of India, for a J. C. Bose fellowship. B.V. and V.S.N. thank the CSIR, Government of India, for research fellowships.

Keywords: carbon nanotubes · CD spectroscopy · chirality · self-assembly · π-gelators

How to cite: *Angew. Chem. Int. Ed.* **2016**, *55*, 10345–10349
Angew. Chem. **2016**, *128*, 10501–10505

[1] M. Gardner, *The New Ambidextrous Universe*: *Symmetry and Asymmetry from Mirror Reflections to Superstrings*, 3rd ed., Dover, New York, **2005**.

[2] a) R. Vallery-Radot, E. E. P. Hamilton, L. Pasteur, *Louis Pasteur*: *His Life and Labours*, D. Appleton, New York, **1886**; b) S. F. Mason, *BioSystems* **1987**, *20*, 27–35; c) A. Brack, *NATO ASI Ser. Ser. C* **1993**, *416*, 345–355.

[3] J. Bailey, *Origin Life Evol. Biospheres* **2001**, *31*, 167–183.

[4] a) C. Velasco-Santos, A. L. Martinez-Hernández, A. Consultchi, R. Rodriguez, V. M. Castaño, *Chem. Phys. Lett.* **2003**, *373*, 272–276; b) K. J. MacKenzie, C. See, O. M. Dunens, A. T. Harris, *Nat. Nanotechnol.* **2008**, *3*, 310–310.

[5] a) D. M. Guldi, G. M. A. Rahman, F. Zerbetto, M. Prato, *Acc. Chem. Res.* **2005**, *38*, 871–878; b) T. Nakanishi, T. Michinobu, K. Yoshida, N. Shirahata, K. Ariga, H. Möhwald, D. G. Kurth, *Adv. Mater.* **2008**, *20*, 443–446; c) A. Llanes-Pallas, K. Yoosaf, H. Traboulsi, J. Mohanraj, T. Seldrum, J. Dumont, A. Minoia, R. Lazzaroni, N. Armaroli, D. Bonifazi, *J. Am. Chem. Soc.* **2011**, *133*, 15412–15424; d) J. M. Malicka, A. Sandeep, F. Monti, E. Bandini, M. Gazzano, C. Ranjith, V. K. Praveen, A. Ajayaghosh, N. Armaroli, *Chem. Eur. J.* **2013**, *19*, 12991–13001; e) S. S. Babu, V. K. Praveen, A. Ajayaghosh, *Chem. Rev.* **2014**, *114*, 1973–2129; f) J. López-Andarias, J. L. López, C. Atienza, F. G. Brunetti, C. Romero-Nieto, D. M. Guldi, N. Martín, *Nat. Commun.* **2014**, *5*, 3763; g) W. Nakanishi, K. Minami, L. K. Shrestha, Q. Ji, J. P. Hill, K. Ariga, *Nano Today* **2014**, *9*, 378–394; h) S. Marchesan, M. Prato, *Chem. Commun.* **2015**, *51*, 4347–4359; i) F. Tsuyohiko, N. Naotoshi, *Sci. Technol. Adv. Mater.* **2015**, *16*, 024802.

[6] a) S. Srinivasan, S. S. Babu, V. K. Praveen, A. Ajayaghosh, *Angew. Chem. Int. Ed.* **2008**, *47*, 5746–5749; *Angew. Chem.* **2008**, *120*, 5830–5833; b) S. Srinivasan, V. K. Praveen, R. Philip, A. Ajayaghosh, *Angew. Chem. Int. Ed.* **2008**, *47*, 5750–5754; *Angew. Chem.* **2008**, *120*, 5834–5838.

[7] a) A. R. A. Palmans, J. A. J. M. Vekemans, E. E. Havinga, E. W. Meijer, *Angew. Chem. Int. Ed. Engl.* **1997**, *36*, 2648–2651; *Angew. Chem.* **1997**, *109*, 2763–2765; b) J. H. K. K. Hirschberg, L. Brunsveld, A. Ramzi, J. A. J. M. Vekemans, R. P. Sijbesma, E. W. Meijer, *Nature* **2000**, *407*, 167–170; c) M. A. Mateos-Timoneda, M. Crego-Calama, D. N. Reinhoudt, *Chem. Soc. Rev.* **2004**, *33*, 363–372; d) A. Ajayaghosh, R. Varghese, S. J. George, C. Vijayakumar, *Angew. Chem. Int. Ed.* **2006**, *45*, 1141–1144; *Angew. Chem.* **2006**, *118*, 1159–1162; e) A. Ajayaghosh, R. Varghese, S. Mahesh, V. K. Praveen, *Angew. Chem. Int. Ed.* **2006**, *45*, 7729–7732; *Angew. Chem.* **2006**, *118*, 7893–7896; f) S. Ghosh, X. Q. Li, V. Stepanenko, F. Würthner, *Chem. Eur. J.* **2008**, *14*, 11343–11357; g) T. Yamamoto, T. Fukushima, A. Kosaka, W. Jin, Y. Yamamoto, N. Ishii, T. Aida, *Angew. Chem. Int. Ed.* **2008**, *47*, 1672–1675; *Angew. Chem.* **2008**, *120*, 1696–1699; h) T. E. Kaiser, V. Stepanenko, F. Würthner, *J. Am. Chem. Soc.* **2009**, *131*, 6719–6732; i) M. Liu, L. Zhang, T. Wang, *Chem. Rev.* **2015**, *115*, 7304–7397; j) L. Zhang, T. Wang, Z. Shen, M. Liu, *Adv. Mater.* **2016**, *28*, 1044–1059.

[8] A. Ajayaghosh, C. Vijayakumar, R. Varghese, S. J. George, *Angew. Chem. Int. Ed.* **2006**, *45*, 456–460; *Angew. Chem.* **2006**, *118*, 470–474.

[9] a) M. J. O'Connell, S. M. Bachilo, C. B. Huffman, V. C. Moore, M. S. Strano, E. H. Haroz, K. L. Rialon, P. J. Boul, W. H. Noon, C. Kittrell, J. Ma, R. H. Hauge, R. B. Weisman, R. E. Smalley, *Science* **2002**, *297*, 593–596; b) T. Fukushima, A. Kosaka, Y. Ishimura, T. Yamamoto, T. Takigawa, N. Ishii, T. Aida, *Science* **2003**, *300*, 2072–2074; c) V. C. Moore, M. S. Strano, E. H. Haroz, R. H. Hauge, R. E. Smalley, J. Schmidt, Y. Talmon, *Nano Lett.* **2003**, *3*, 1379–1382.

[10] a) M. M. J. Smulders, M. M. L. Nieuwenhuizen, T. F. A. de Greef, P. van der Schoot, A. P. H. J. Schenning, E. W. Meijer, *Chem. Eur. J.* **2010**, *16*, 362–367; b) P. A. Korevaar, S. J. George, A. J. Markvoort, M. M. J. Smulders, P. A. J. Hilbers, A. P. H. J. Schenning, T. F. A. De Greef, E. W. Meijer, *Nature* **2012**, *481*, 492–496.

Received: June 1, 2016
Published online: July 27, 2016

